

ANSA AS AN ADVANCED TOOL IN BIOMEDICAL MODELLING AND ENGINEERING

¹A. Tsouknidas[▲], ²S. Savvakis, ³N. Michailidis, ⁴K. Anagnostidis

¹Laboratory for Machine Tools and Manufacturing Engineering, Mechanical Engineering Department, Aristotle University of Thessaloniki, Greece, ²Laboratory of Applied Thermodynamics, Mechanical Engineering Department, Aristotle University of Thessaloniki, Greece, ³Physical Metallurgy Laboratory, Mechanical Engineering Department, Aristotle University of Thessaloniki, Greece, ⁴3rd Orthopaedic Department "Papageorgiou" General Hospital, Aristotle University of Thessaloniki, Greece

KEYWORDS – Biomedical modelling, Reverse engineering, Anatomic specific mesh generation

ABSTRACT – 3-D finite element models representing functional parts of the human body have been repeatedly introduced over the last years in order to simulate the biomechanical response of the human musculoskeletal system or investigate trauma related surgical treatment.

The first part of this study introduces ANSA as a Finite Element Analysis (FEA) based tool for the manipulation and segmentation of Computer Tomography (CT) based data, to obtain a geometrically accurate representation of a human skull and lumbar spine segment respectively.

In a second approach a mixed element technique was applied during the mesh generation of the lumbar spine segment, facilitating the construction of compound-elements which allow for the consideration of complex anatomical characteristics, such as the anisotropy of the intervertebral discs. This provided valuable insight on the stress development within the model under multi-axial loading.

The novelty of the introduced model is based on the anatomical specific mesh generation, incorporating anatomic details of the examined tissue during modelling (pre-processor) in contrast to hitherto presented models considering anisotropic material properties solely during the simulation itself (post-processor). This results in smooth stress transitions among the individual model units and superior results' accuracy.

TECHNICAL PAPER -

1. INTRODUCTION

Three dimensional finite element models representing functional parts of the human musculoskeletal system have been repeatedly introduced over the last years. Such models cover a wide spectrum of applications, simulating among others the stress transition between endosteal implants and vicinal bone tissue (Lin et al., 2010, Jung et al. 2008, Yokoyama et al., 2004), the biomechanical response of spinal units (Little et al, 2010, Ezquerro et al, 2004, Wang et al, 2006) or investigate trauma related surgical treatment (Polikeit et al, 2003, Ashish and Pramod 2009) etc.

Several methods have been employed to obtain the desired geometrical characteristics and even though touch probe digitizers (Lee et al, 2002) and laser scanners (Heuer et al, 2007) are able to provide high accuracy measurements, thus leading to accurate 3D representations, non intrusive methods such as CT (Kinder et al, 2009) or Magnetic Resonance Imaging (MRI) (Pfirrmann, et al, 2001) ease the extraction of the geometric information while comparing favourably in terms of data processing and inherent defect determination.

These advantages render computer tomography as the imaging technique of choice due to its ability to demonstrate high inherent image contrast between bone and soft tissue. This enables relatively unhindered segmentation of the bone from soft tissue, allowing the generation of a geometrically accurate volumetric data set of the patient's head. The basic concept is to overlay CT scan slices, which represent the outline of the examined bone

fragment (Pahr and Zysset, 2009, Blankevoort et al, 2008, Beimersade et al, 2008, Kobayashi et al, 2009).

Recent studies have used combinations of the above techniques to simulate parts of the human spine ranging from a set of vertebra (Lodygowski et al, 2005) up to several parts of the spine (Guan et al, 2006).

The acquisition of the geometrical characteristics of hard tissue is however the first step in a series of processes required to set-up a model that can be further on employed to determine some of the human musculoskeletal systems' characteristics. The following step, and even more demanding aspect concerning the accuracy of the final model, lies within the mesh generation of these complex geometries and is an essential aspect of biomedical modelling. All above referenced publications use the solvers automated mesh generator to define the numerical grid and consider anatomical characteristics in the elements employed during the simulation. Although this is a proven technique and should not be discredited, it provides limited quality in the calculated stress distributions while different solvers will require different mesh densities to achieve mesh independent grid.

In this study, the pre-processor ANSA developed by BETA CAE Systems was used to generate the meshing of a traumatized human skull, directly following the extraction of its geometrical characteristics based on CT measurements. Prior to the mesh generation, the ANSA TOPO menu was employed to reconstruct its partially fractured anatomy.

In a second approach, the same software is introduced as a novel tool to consider the anatomical characteristics of a spine segment during the mesh generation and facilitate the usage of compound elements used to consider several innovative bio related aspects.

2. MESH GENERATION FOR APPLICATIONS IN CRANIOPLASTY

Alloplast cranial implants must satisfy several important criteria, such as biocompatibility, customized geometry to ensure direct contact with bone tissue and sufficient mechanical properties to withstand functional related stress.

In the present study the mechanical behaviour of reverse engineered and rapid prototyped Polymethylmethacrylate (PMMA) and Titanium (Ti) alloy cranial implants is examined and their capacity to absorb impact forces evaluated, considering the developing stress fields of the implant and vicinal bone tissue. The overall neurocranial protection provided by both implants will also be assessed and the maximum applicable force determined. This is facilitated though the application specific mesh generation of both, skull and implant geometry.

Implant design

The procedure of manufacturing customized cranial implants through CAD/CAM assisted techniques is usually referred to as Computer Assisted Cranioplasty (CAC) and is as already mentioned, predominantly based on CT measurements of the patients skull.

During the present investigation an entire cranial defect was scanned from below its lower boundaries to its upper limit ensuring the full 3D visual representation of the trauma.

Data acquisition was in accordance with DICOM (Digital Imaging and Communications in Medicine) and interpolation of the CT information ensured an isotropic data set. Although this process did not indicate higher resolution of the reconstructed skull, it led to a smoother representation allowing the distinct removal of the soft tissue in close proximity to the contour at the defect edge.

The modelling of the cranial surface is an automated process following the bone segmentation mentioned above. A 3D surface of the skull investigated as well as the lateral trauma can be seen in figure 1. The representation shows the skull volume obtained through the CT imaging technique.

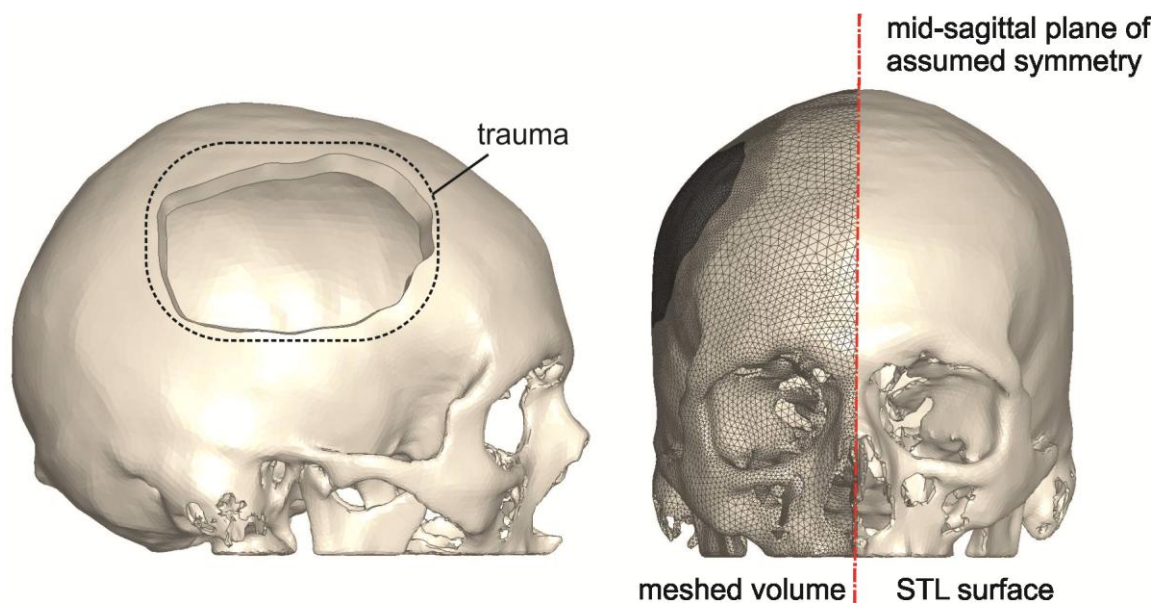


Figure 1 – CT assisted 3D representation of the traumatized skull, surface and meshed model of the skull and implant

In order to design a custom implant based on the individual anatomy and to ensure an acceptable cosmetic outcome, the patient's skull was assumed to be symmetrical along its mid-sagittal plane as shown in the right part of figure 1, the right part of which represents the skull geometry as received by the CT measurements whereas the left part incorporates the meshing of skull and implant.. This facilitated the replication of the missing bone fragment from a mirrored volume of the contra-lateral side of the skull (Winder et al,2006).

The contour profile of the implant was obtained through a projection of the defect edge curvature on the mirrored data set, which ensured a perfect fitting of the implant edges on the defected bone tissue, as illustrated in figure 1.

FEM model

The CT generated geometry of the skull and implant was used to create a FEM model and the corresponding simulation software used was ANSYS WORKBENCH (ANSYS Inc. Canonsburg, USA). The FEM model facilitates the three-dimensional stress - strain analysis of the implant as well as the surrounding bone tissue of the skull caused by the application of a specific load. The reference load was 100N, while a further load of 1780N was applied, simulating the impact of a tennis ball at an average speed of 30m/s (Allen et al, 2008). The load was applied horizontally and was evenly distributed over an area of approximately 3 mm² at the centre of the implant, as shown in figure 2. The model was bound at the upper part of the atlas and no contact was assumed between the cranium and implant except at the fixation points.

The meshing of the examined surfaces was conducted in ANSA of BETA CAE Systems in order to ensure a proper element size leading to a realistic and isotropic stress transition within the implant material and bone tissue. The resulting maximum and minimum element size as well as the number of elements for each part considered are demonstrated in Table 1.

Element type	no. of Elements	max size Element	min size Element
Skull	535771	6,78 mm	0,11 mm
Implant	28506	4,34 mm	0,66 mm
Fixation plates	1305	2,17 mm	0,63 mm

Table 1 - Mesh related figures.

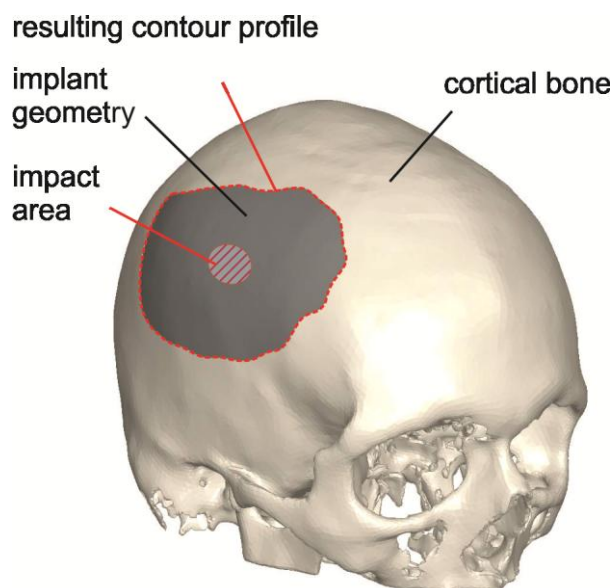


Figure 2 – Implant design by means of Computer Assisted Cranioplasty

Figure 2 illustrates the full extent of the trauma, filled with a PMMA implant. In both material cases the implant was stabilized by titanium (Ti6Al4V) plates. The model was then imported into ANSYS® Academic Research, Release 12.1 for the finite element simulation.

The mechanical properties of the cortical and cancellous bone tissue were considered to be linear and isotropic according to Table 2 (Wang and Yang, 2010).

Material	Modulus of Elasticity [MPa]	Poisson's ratio
Cortical bone	15.000	0,3
Cancellous bone	500	0,3
Ti6Al4V	113.800	0,342
PMMA	2.944	0,375

Table 2 - Mechanical properties of implant material and bone tissue.

Mechanical strength

Through the visualization of the developing stress – strain distributions the critically affected regions can be determined and the eventual failure of the alloplast implant predicted.

The reference force of 100N was absorbed by both implant materials without the development of unsettling stress or strain neither on the implant nor on the cranium. The maximum stress developed on the Ti-alloy and PMMA implant were 8,163MPa and 2,88MPa respectively, while the resulting highest cranial stress developed was observed in both cases near the contact region of the implant with the skull, corresponding to 5,23MPa for the Ti-alloy implant and 8,44MPa for the PMMA implant.

In both cases, the impact load of 1780N developed stresses indicating the same critical region as for the aforementioned load. Even though both implants are able to endure the resulting stress, their varying elasticity modulus and deformation generated different reactions on the bone tissue, which in the case of the PMMA implant was barely able to withstand the load applied, while the Ti-alloy implant did not cause critical stress distributions within its close vicinity. The highest stresses developed on the cranium were increased for the model concerning the PMMA implant, with upper limits of 150,15 MPa, while in the case of the Ti-alloy implant they were limited to 93,11 MPa.

The developed model was further on employed to determine the mechanical behaviour of both implants for various loads. The maximum developing von Mises stress for both material cases versus the applied load is presented in figure 3. The initiation of the dashed

part of the PMMA curve corresponds to the maximum stress, which exceeds the mechanical strength of the materials studied, indicating the maximum static force that can be applied. In the case of the Ti6Al4V, which is an implant that can endure up to 950 MPa, the fracture point of the implant was not reached in either of the cases examined. The linear tendency of both curves can be attributed to the linear elastic constitutive law which was employed during all simulations.

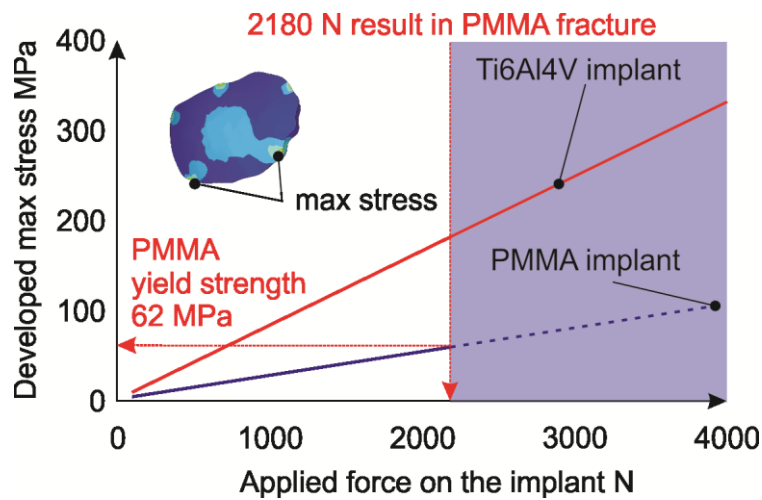


Figure 3 – Maximum developing von Mises stress for Ti6Al4V and PMMA implant versus the applied load

Shock resistance

The stress distribution in both cases was localized in the same skull region. This was expected, since the constitutive equation, skull and implant geometry, bone properties and boundary conditions used were identical in all cases examined. However, it is important to take into consideration also the biomechanical response of the implant material and the bone for the impact of the applied load (Masson et al, 2010).

Although it was anticipated that the Ti-alloy implant can withstand higher loads, due to its higher mechanical properties, it is highly interesting that it absorbs these loads in a far better way compared to the PMMA implant, thus leading to lower stress fields in the critical regions. The deformation of the PMMA implant was twice than that exhibited by the Ti-alloy implant, thus forcing itself onto the bordering bone which developed stresses close to its yield strength, which rendered the contact area as critical. A direct comparison of the stressed cranium using PMMA and Ti-alloy implants in the critical contact region can be observed in figure 4.

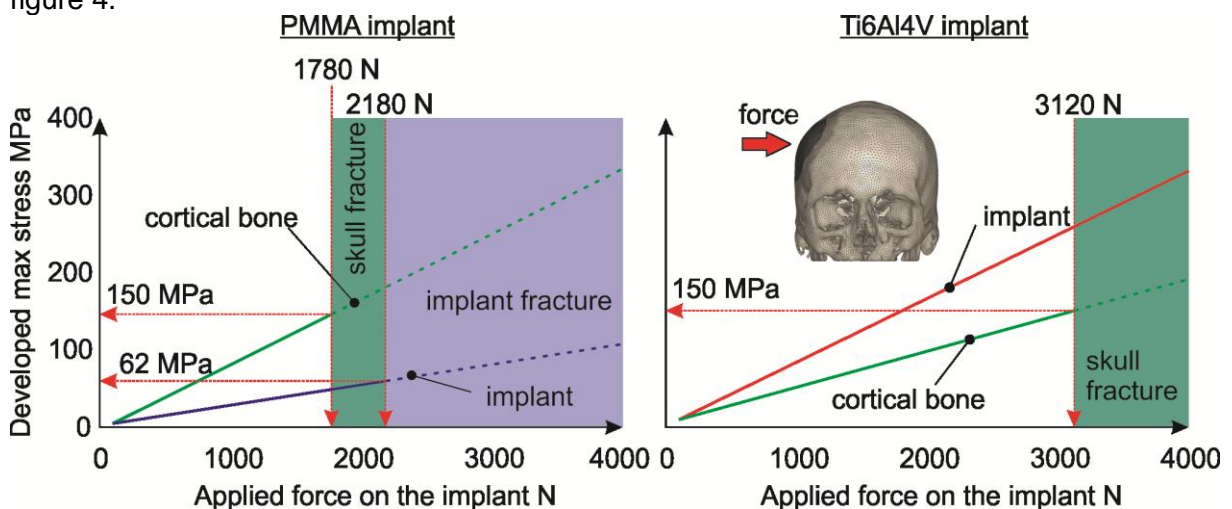


Figure 4 – Maximum developing von Mises stress on the cortical bone and implant versus the applied load for both implant materials

The growth rate of developing maximum stress within the cortical bone as a function of the applied force was once again linear, due to the linear elastic constitutive law considered. Figure 4 exhibits this behaviour for both implants while the yield strength of the bone tissue is defined as the transition point of the continuous line to the dashed line. The shaded area of both diagrams presented in figure 4 indicates forces that would result in fracture of the skull under the corresponding load, 1780 MPa and 3120 MPa in the case of PMMA and Ti-alloy respectively. Although the behaviour of the cancellous bone was taken into account during the simulation, it was not considered as a fracture criteria due to the superior mechanical strength properties of the cortical bone.

Critical deflection

Another crucial parameter directly affected by the differing behaviour of both materials is the deflection of the implant. Since the implant is placed in close proximity to the patient's meninges and brain, it is imperative to avoid neurocranial damage inflicted by the deforming implant. During the load examined, the implant material inertial comes in contact with the meninges causing an increase in brain pressure. This, in conjunction with the occurred deflection, will induce further stress on the brain tissue associated with contusions and other neurocranial traumas (Van Dommelen et al, 2010, Fujiwara et al, 1989). The calculated deflection over the critical cross-section of the implant of both materials (Ti6Al4V and PMMA) is shown in figure 5. It is notable that the highest deflection does not occur in the same position for both implants and neither does it bear the same directionality. The Ti-alloy, due to its significantly higher elasticity modulus, develops increased stress distributions in the impact area compared to the PMMA implant, but exhibits deflections of approximately half the magnitude of those of the PMMA implant. Furthermore, these stresses appear within its concave geometry and not on its perimeter, as in the case to the PMMA implant, thus providing far superior neurocranial protection.

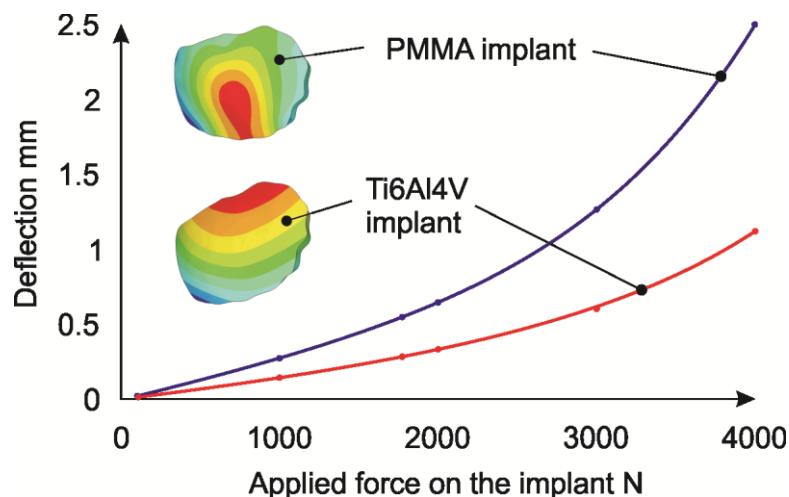


Figure 5 – Critical deflection of Ti6Al4V and PMMA implant

3. ANATOMICAL SPECIFIC MESH GENERATION OF A FUNCTIONAL SPINE UNIT

The second chapter of this study presents a CT based FEM model of the lumbar spine taking into account all function related boundary conditions such as anisotropy of mechanical properties, ligaments, contact elements mesh size etc. The introduced anatomical specific mesh generation as well as the usage of compound elements represent the novelist of this study. Several innovative aspects that have been separately considered in previous studies, like material specific properties (unequal properties distribution among annulus fibrosus layers, directional bone anisotropy etc.) and all connective tissue (ligament long anterior, ligament long posterior, ligament supraspinalia etc.) were also considered. All these aspects,

combined in a high accuracy CT based model of a Functional Spine Unit (FSU), facilitate the simulation of complex loading scenarios in a far more accurate way than before, while the introduced approach can be extended to the entire human spine.

Method

During the reconstruction of the FSU (L1-L2 of the lumbar spine) CT measurements were employed and data acquisition was once again in accordance to DICOM.

After the representation of the vertebrae outer surfaces the bone types were segmented considering an outer cortex for each vertebra corresponding to the cortical bone with a shell thickness of 0.5, resulting by offsetting the outer vertebral surface. The remaining volume of each vertebra was considered as cancellous bone and described as such in the way illustrated in figure 6.

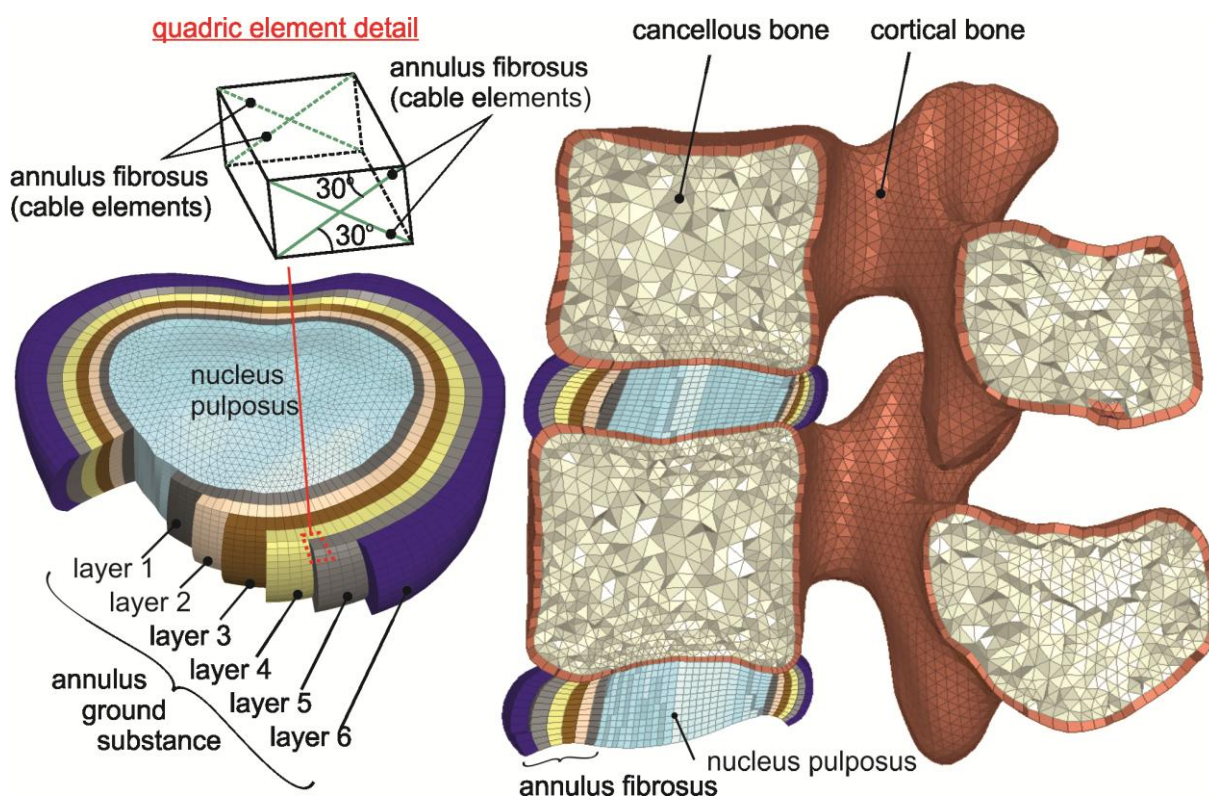


Figure 6 – Resulting mesh of the L1-L2 vertebra with cortical and cancellous bone allocation and reverse engineered intervertebral disc with nucleus pulposus and the surrounding annulus ground substance.

Unlike the aforementioned procedure, the intervertebral discs of the lumbar spine were reverse engineered based on the superior and inferior surface of the connecting vertebral bodies. This method compares favourably to the regeneration of the discs based on CT measurements due to the fact that their volume is characterized by severely altering density and this inhomogeneous tissue does not facilitate precise segmentation by imaging techniques. The geometric characteristics of the intervertebral discs were designed based on the existing spinal bone tissue, while anatomic data like the inner nucleus pulposus and the surrounding outer annulus were considered. The resulting meshed geometry of every intervertebral disc (shown in figure 6) consists of six spline based layers, proportional concentric to the outer contour of the disc, covering a total of 65% of the discs superior and inferior surface.

In order to determine the optimum mesh density in terms of processing time, with regard to the results accuracy as well as the element aspect ratio and size increase towards the vertebra centre (cancellous bone), convergence studies were conducted for every vertebra and intervertebral disc individually.

During the mesh generation of the intervertebral disc, a mixed element technique was applied to facilitate the construction of compound-elements for the annulus ground substance. Quadric elements were employed for the annulus ground substance (primary element) in order to facilitate the implementation of the annulus fibrosus in form of cable elements (secondary elements) positioned crosswise within the tetrahedron structure. The resulting compound-element allows for the accurate simulation of the intervertebral discs' biomechanical response, as this approach ensures directional dependent stiffness and absorption of torsion related loads. Approximately 2000 such elements were employed for each intervertebral disc (depending on disc size) exhibiting 30 degrees angle to the top and bottom surface of the elements (as shown in the quadric element detail of figure 6).

The remaining model, nucleus pulposus and vertebrae, composes of tetrahedral elements (pyramides) and the unhindered connection at the models contact areas (quadric- tetra elements interface) was ensured through the diametrical incision of two triangles in every rectangle, maintaining the same nodes throughout the intervertebral disc surface and the vicinical vertebrae. This approach obviated the usage of contact elements, thus reducing the processing time of the FEM model.

The mechanical properties of cortical and cancellous bone were considered as anisotropic (Lu and Hutton, 1996, Smit et al, 1997) and are presented in table 3 along with the strength characteristics of the nucleus pulposus and the of the annulus ground substance of the intervertebral discs.

Material type	Young modulus [Mpa]	Poisson ratio	Employed element type
Cortical bone	$E_{xx} = 11.300$	$\nu_{xy} = 0,484$	solid 185
	$E_{yy} = 11.300$	$\nu_{yz} = 0,203$	
	$E_{zz} = 22.000$	$\nu_{xz} = 0,203$	
	$G_{xy} = 3.800$		
	$G_{yz} = 5.400$		
	$G_{xz} = 5.400$		
Cancellous bone	$E_{xx} = 140$	$\nu_{xy} = 0,45$	solid 95
	$E_{yy} = 140$	$\nu_{yz} = 0,315$	
	$E_{zz} = 200$	$\nu_{xz} = 0,315$	
	$G_{xy} = 48,3$		
	$G_{yz} = 48,3$		
	$G_{xz} = 48,3$		
Nucleus pulposus	0,2	$\nu = 0.4999$	solid 185
Annulus ground substance	4,2	$\nu = 0.45$	solid 185

Table 3 - Material properties and element specifications of cortical and cancellous bone as well as nucleus pulposus and annulus ground substance.

Among the most important characteristics of the FEM model was the incorporation of a set of cable elements, adding valuable mechanical characteristics to the simulation. The annulus fibrosus was considered to exhibit varying young modulus for each set of layer in the radial direction of the annulus (as presented in figure 6) in order to reflect the unequal distribution of this structures properties. Next to these, several other cable elements were employed representing the remaining connective tissue between each set of vertebrae, thus ensuring the precise transition of forces among the vertebra and simulating the accurate biomechanical response of the lumbar spine.

Figure 7 (left part) demonstrates all aforementioned connections (ligaments, contact elements and annulus fibrosus) used as input to the FEM software (ANSYS 12.1 Academic

license) as well as a simplified model (right part of same figure) illustrating only the cable and contact elements considered during the simulation.

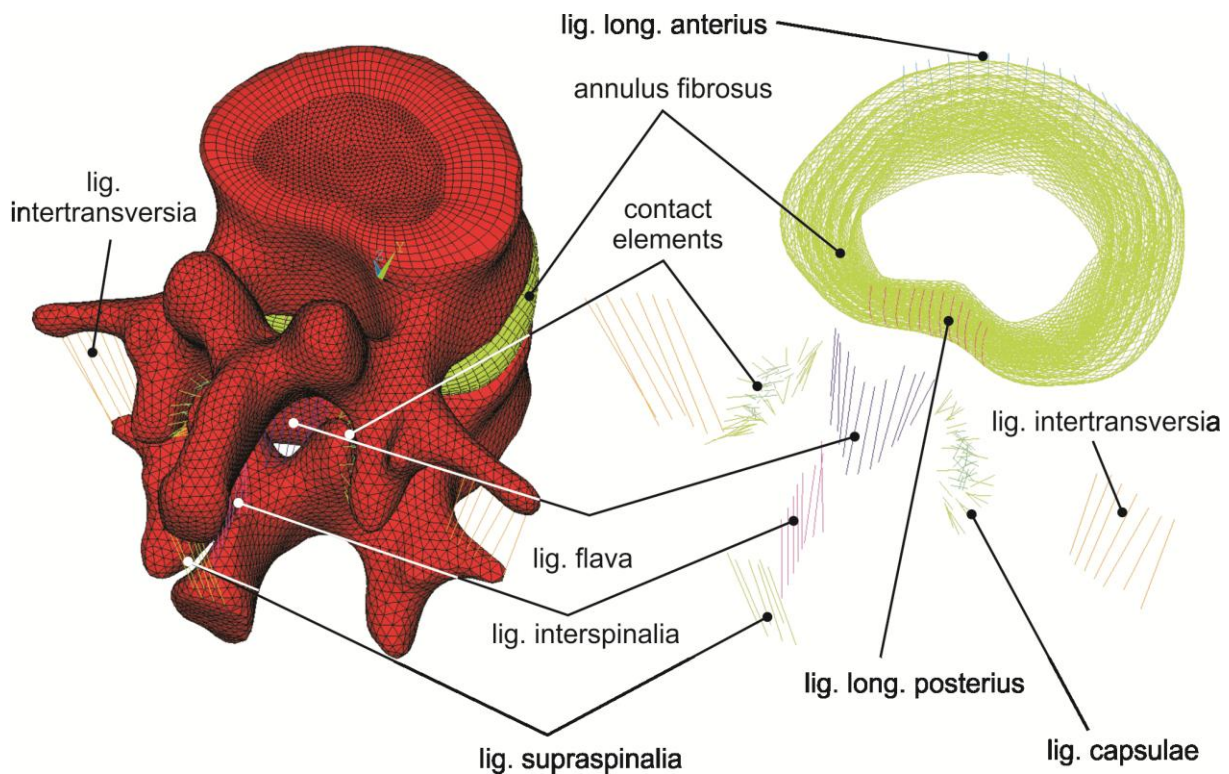


Figure 7 – a) Set of two vertebrae (L1 and L2), intervertebral disc and ligaments b) simplified model without bone and tissue presenting only ligaments and contact elements.

The mechanical properties as well as the cross sectional area of each cable element used within the model (Shirazi-ald et al, 1984, Smit et al, 1997, Lu and Hutton, 1996) are presented in table 4.

Cable element type	Young modulus [Mpa]	Poisson ratio	Cross-sectional area [mm ²]
Lig. long. anterior	20	0,3	38
Lig. long. Posterior	70	0,3	20
Lig. flava	50	0,3	60
Lig. intertransversaria	50	0,3	10
Lig. interspinalia	28	0,3	35,5
Lig. supraspinalia	28	0,3	35,5
Lig. capsulae	20	0,3	40
Annulus fibr. layer 1	550	0,45	0,7
Annulus fibr. layer 2	495	0,45	0,63
Annulus fibr. layer 3	440	0,45	0,55
Annulus fibr. layer 4	420	0,45	0,49
Annulus fibr. layer 5	385	0,45	0,41
Annulus fibr. layer 6	360	0,45	0,3

Table 4 - Mechanical properties of ligaments, contact elements and annulus fibrosus layers.

All cable elements were simulated with ANSYS “link 10” elements which are capable of receiving only tension loads resembling the ligaments in a rather accurate way and mimicking the torsional resistance of the lumbar spine (annulus fibrosus).

The meshing of the volume presented in figure 6 was conducted in ANSA in order to ensure all above mentioned characteristics leading to a realistic and isotropic stress

transition within the considered bone and intervertebral disc. The resulting maximum and minimum element size as well as the number of elements for each set of material considered are demonstrated in table 5.

Material type	no. of Elements	max Element side length	min Element side length
Cortical bone	17.504	0,24 mm	0,38 mm
Cancellous bone	203.677	4,75 mm	0,38 mm
Nucleus pulposus	6.636	1.99mm	0.34mm
Annulus	12.612	3.10mm	0.19mm

Table 5 - Mesh related figures of the FSU model.

Results

The introduced FEM model was employed to determine the stress fields resulting from a 150 N compression load subjected to a further torsion of 10 Nm. The upper left side of the figure demonstrates the equivalent stress distribution of the cortical bone mass, while the right part of the same figure visualizes the corresponding the stress fields for the cancellous bone.

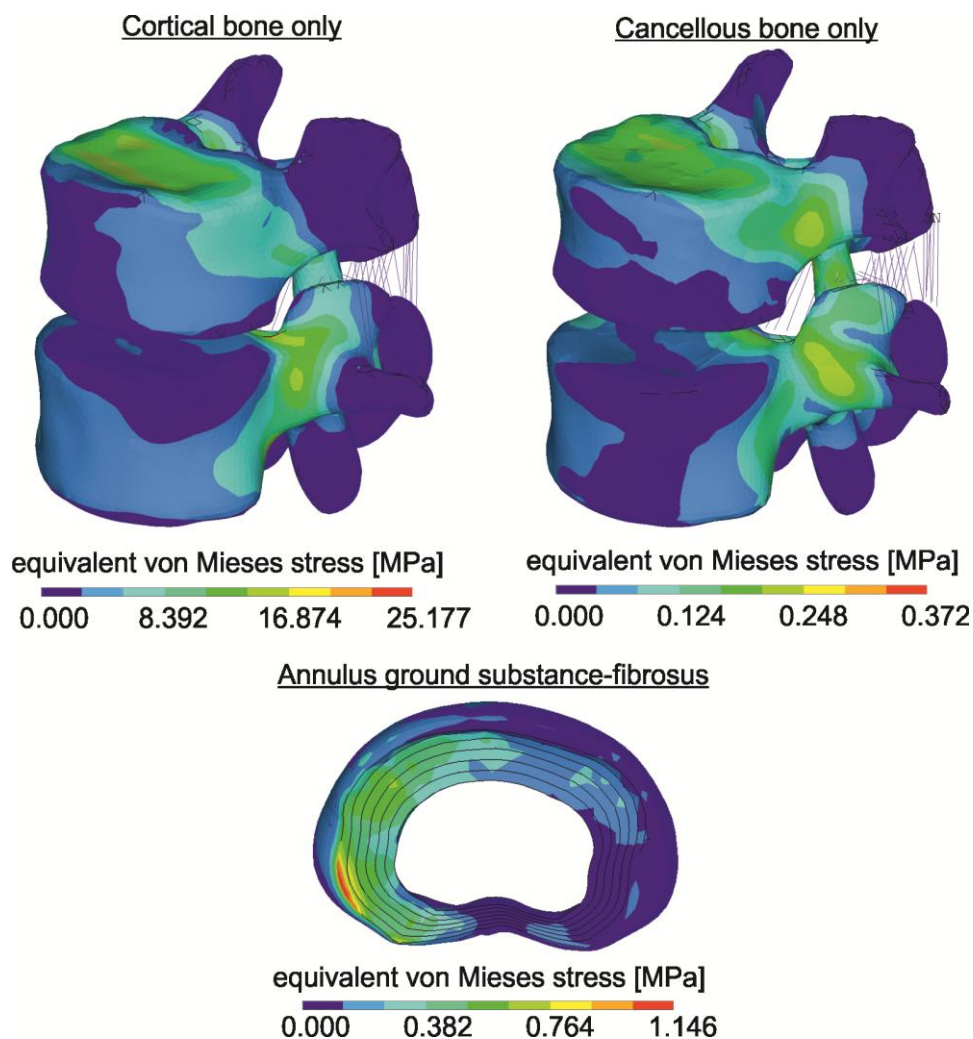


Figure 8 – Calculated stress distribution on cortical-, cancellous bone matter and intervertebral disc.

Although both cortical and cancellous bone exhibit almost identical stress distributions, the maximum stresses differ by two magnitudes (25.177 MPa for the cortical bone and 0.372 MPa for the cancellous bone). This was however to be expected because the materials young modulus present a similar aberration: 11.300 MPa for the cortical bone and 140 MPa for the cancellous bone (both in the XX direction). Furthermore, the stresses developed in both cases are below the bones' fracture strength.

In order to accurately assess the biomechanical response of the functional spine unit, numerically obtained by the introduced FEM technique, several spine segments and individual vertebral bodies and intervertebral discs were subjected to compressive loads, in order to monitor their deformation and compare the experimental values to the analytical obtained ones. The results were presented elsewhere (Tsouknidas et al, 2011) and exhibited excellent convergence sustaining the adequacy of the introduced technique.

4. CONCLUSIONS

ANSA of BETA CAE Systems can be successfully employed in biomedical engineering, not only as a Mesh Generator ensuring a proper finite element analysis which determines a realistic and isotropic stress transition, but also as a CAD Tool (TOPO menu) for fixing the initial geometry, as presented in the first part of this investigation.

The adequacy of PMMA and Ti-alloy implants to withstand normal - everyday loads is well proven by their wide use in craniofacial reconstruction. Even though PMMA cannot withstand forces endured by Ti alloys, its mechanical strength is sufficient to tolerate higher loads than the vicinal bone tissue (figure 4) thus providing sufficient neurocranial protection in terms of fracture strength. Nevertheless, the Ti-alloy implant compared favourably in terms of shock resistance not only absorbing higher amounts of energy, but also leading to lower stress fields in close proximity to the skull defected edge. The main advantage however exhibited by the Ti6Al4V is its significantly lower deflection, compared to the loaded PMMA implant, which under critical loads may cause indentations of the implant up to 1.2mm (figure 5) deep into the brain.

The FEM modelling technique introduced in the second section of this paper can be used for the reconstruction of any spine segment allowing the consideration of complex material properties (anulus fibrosus etc.) in order to accurately resemble the spines' biomechanical response under various loading conditions. The validation of the model was achieved based on cadaveric experiments as well as literature data and it was considered as highly accurate in the case of single loading conditions.

5. ACKNOWLEDGMENTS

The authors would like to thank BETA CAE Systems SA for providing them with the CAE pre-processor ANSA used during surface generation and volume meshing of the cranium and the FSU.

6. REFERENCES

- (1) Lin D, Li Q, Li W, Duckmanton N, Swain M, 2010, Mandibular bone remodeling induced by dental implant. *J Biomech.* 43(2):287-93.
 - (2) Jung RE, Pjetursson BE, Glauser R, Zembic A, Zwahlen M, Lang NP, 2008, A systematic review of the 5-year survival and complication rates of implant-supported single crowns. *Clin. Oral Impl. Res.* 19: 119-130.
 - (3) Yokoyama S, Wakabayashi N, Shiota M, Ohyama T, 2004, The influence of implant location and length on stress distribution for three-unit implant-supported posterior cantilever fixed partial dentures. *J Prosthet Dent.*, 91(3):234-40.
-

- (4) Little, J.P., Pearcy, M.J., Tevelen, G., Evans, J.H., Pettet, G., Adam, C.J., 2010. The mechanical response of the ovine lumbar anulus fibrosus to uniaxial, biaxial and shear loads. *Journal of the Mechanical Behavior of Biomedical Materials*, 3, 146-157
 - (5) Ezquerro, F., Simón, A., Prado, M., Pérez, A., 2004. Combination of finite element modeling and optimization for the study of lumbar spine biomechanics considering the 3D thorax–pelvis orientation. *Medical Engineering & Physics*, 26(1), 11-22
 - (6) Wang, J.P., Zhong, Z.C., Cheng, C.K., Chen, C.S., Yu, C.H., Chang, T.K., Wei, S.H., 2006. Finite element analysis of the spondylolysis in lumbar spine. *Biomedical Materials Engineering* 16(5), 301-308.
 - (7) Polikeit, A., Ferguson, S.J., Nolte, L.P., Orr, T.E., 2003. Factors influencing stresses in the lumbar spine after the insertion of intervertebral cages: finite element analysis. *European Spine Journal*, 12(4):413-20
 - (8) Ashish, D., Pramod, P., 2009. Development of Computer Aided 3D Model From Computed Tomography Images and its Finite Element Analysis for Lumbar Interbody Fusion with Instrumentation. *International Journal of CAD/CAM* 9(1) 121-128
 - (9) Lee, K.K. Teo, E.C. Qiu, T.X. Ng, H.W. and Yang, K., 2003. Finite element modeling of L2-L3 using digitizer. *International Journal of Computer Applications in Technology (Special issue on Biomedical Engineering and I.T.)* 20 1-9
 - (10) Heuer, F., Schmidt, H., Claes, L., Wilke, H.J., 2008. A new laser scanning technique for imaging intervertebral disc displacement and its application to modeling nucleotomy. *Arthroscopy: The Journal of Arthroscopic and Related Surgery* 23(3) 260-269
 - (11) Klinder, T., Ostermann, J., Ehm, M., Franz, A., Kneser, R., Lorenz, C., 2009. Automated model-based vertebra detection, identification, and segmentation in CT images. *Medical Image Analysis* 13, 471–482
 - (12) Pfirrmann, C., Metzdorf, A., Zanetti, M., Hodler, J., Boos, N., 2001. Magnetic Resonance Classification of Lumbar Intervertebral Disc Degeneration. *Spine* 26(17), 1873–1878
 - (13) Pahr, D.H., Zysset, P.K., 2009. From high-resolution CT data to finite element models: development of an integrated modular framework. *Comput Methods Biomech Biomed Engin.* 12(1), 45-57.
 - (14) Blankevoort, L., Beimers, L., Jonges, R., Valstar, E.R., Tuijthof, G.J.M., 2008. The accuracy of a CT-based bone segmentation technique for measuring the range of motion of the joints in the ankle. *J. Foot Ankle Res.* 1, O34
 - (15) Beimersade, L., Tuijthofde, G.J.M., Blankevoortde, L., Jonges, R., Maas, M., Van Dijk, C.N., 2008. In-vivo range of motion of the subtalar joint using computed tomography, *J. Biomech.* 41, 1390-1397
 - (16) Kobayashi, K., Odagawa, K., Sakamoto, M., Tanabe, Y., 2009. Accuracy of Single Plane X-Ray Image-Based Technique for Assessment of Knee Kinematics, *Journal of Biomechanical Science and Engineering* 4,192-200
 - (17) Lodygowsky, T., Kakol, W., ierszycki, M., 2005. Three-dimensional nonlinear finite element model of the human lumbar spine segment. *Acta of Bioengineering and Biomechanics* 7(2)
-

- (18) Guan, Y., Yoganandan, N., Zhang, J., Pintar, F., Cusick, J., Wolfla, C., Maiman, D., 2006. Validation of a clinical finite element model of the human lumbosacral spine. *Medical & Biological Engineering & Computing* 44, 633–641
 - (19) Winder, R.J., McKnight, W., Golz, T., Giese, A., Busch, L.C., Wulf, J., 2006. Comparison of custom cranial implant source data: Manual, mirrored and CAD generated skull surfaces. *Cranial & Maxillofacial Workshop, MICCAI, Copenhagen*, 5th October 2006.
 - (20) Allen, T., Goodwill, S., Haak, S., 2008. Experimental Validation of a Tennis Ball Finite-element Model for Different Temperatures, *The Engineering of Sport* 7. 1,125-133
 - (21) Wang, S., Yang, J., 2010. Simulating cranio-maxillofacial surgery based on mixed-element biomechanical modelling. *Comput Methods Biomech Biomed Engin* in press.
 - (22) Masson, C., Baque, P., Brunet, C., 2010. Biomechanical response of impacted bony pelvis: influence of the morphometry and bone density. *Comput Methods Biomech Biomed Engin*. in press
 - (23) Van Dommelen, J.A.W., Van der Sande, T.P.J., Hrapko, M., Peters, G.W.M., 2010. Mechanical properties of brain tissue by indentation: Interregional variation. *J. Mech. Behav. Biomed. Mater.* 3, 158-166.
 - (24) Fujiwara, S., Yanagida, Y., Mizoi, Y., 1989. Impact-induced intracranial pressure caused by an accelerated motion of the head or by skull deformation; an experimental study using physical models of the head and neck, and ones of the skull. *Forensic Sci. Int.* 43,159-169.
 - (25) Lu, Y.M, Hutton, W.C, Gharpuray, V.M., 1996. Do bending, twisting and diurnal fluid change in the disc affect the propensity to prolapse? A viscoelastic finite element model. *Spine*, 21,2570-2579.
 - (26) Smit, T.H., Odgaard, A., Schneider, E., 1997. Structure and function of vertebral trabecular bone. *Spine* 15;22(24), 2823-2833.
 - (27) Shirazi-Adl, S.A., Shrivastava, S.C., Ahmed, A.M., 1984. Stress analysis of the lumbar disc-body unit in compression. A three-dimensional nonlinear finite element study. *Spine* 9(2),120-34
 - (28) Tsouknidas, A., Michailidis, N., Savvakis, S., Anagnostidis, K., Bouzakis, K.D., Kapetanios, G., 2011. A FEM modeling technique to determine the mechanical response of a lumbar spine segment under complex loads, *J. Appl. Biomech.* in press
-